Article:
Alosaimi, M, Lesnic, D and Johansson, BT (2021) Solution of the Cauchy problem for the wave equation using iterative regularization. Inverse Problems in Science and Engineering, 29 (13). pp. 2757-2771. ISSN: 1741-5977

https://doi.org/10.1080/17415977.2021.1949590

Solution of the Cauchy problem for the wave equation using iterative regularization

M. Alosaimi[1,2], D. Lesnic[1,*] and B. T. Johansson[3]
[1]*Department of Applied Mathematics, University of Leeds, Leeds LS2 9JT, UK*
[2]*Department of Mathematics and Statistics, College of Science, Taif University, P.O. Box 11099, Taif 21944, Saudi Arabia*
[3]*Mathematics, ITN, Campus Norrköping, Linköping University, 601 74 Norrköping, Sweden*
E-mails: mmmaal@leeds.ac.uk (M. Alosaimi), amt5ld@maths.leeds.ac.uk (D. Lesnic* corresponding author), tomas.johansson@liu.se (B. T. Johansson)

Abstract. We propose a regularization method based on the iterative conjugate gradient method for the solution of a Cauchy problem for the wave equation in one dimension. This linear but ill-posed Cauchy problem consists of finding the displacement and flux on a hostile and inaccessible part of the medium boundary from Cauchy data measurements of the same quantities on the remaining friendly and accessible part of the boundary. This inverse boundary value problem is recast as a least-squares minimization problem that is solved by using the conjugate gradient method whose iterations are stopped according to the discrepancy principle for obtaining stable reconstructions. The objective functional associated is proved Fréchet differentiable and a formula for its gradient is derived. The well-posed direct, adjoint and sensitivity problems present in the conjugate gradient method are solved by using a finite-difference method. Two numerical examples to illustrate the accuracy and stability of the proposed numerical procedure are thoroughly presented and discussed.

Keywords Cauchy problem; wave equation; conjugate gradient method; regularization; inverse problem

1. Introduction

A plethora of research has been devoted to the study of Cauchy problems for various linear and non-linear models, e.g. [1, 2] for linear and non-linear elliptic equations, and [3] for the heat equation. The Cauchy problems arise in situations in which the aim is to determine the data on a hostile and inaccessible (because of corrosion or cracks, for example) boundary part from measurements of the Cauchy data on the remaining friendly and accessible part of the boundary. These problems inevitably occur in the contexts of many biomedical and engineering fields such as cardiology [4], elasticity [5] and heat transfer [6]. For example, in cardiology physicians aim to identify the electrical potential of the inaccessible heart's surface for diagnostic purposes from measurements of the potential on accessible parts of the human body [4].

Researchers in the field have proposed and successfully applied several analytical and numerical techniques [3, 6–9] for the accurate and stable solutions of Cauchy problems, mostly to elliptic and parabolic models. Bastay et al. [10] proposed and proved the convergence of two iterative methods for the solution of the Cauchy problem for parabolic equations. Hào [3] constructed a gradient-based minimization method for the Cauchy problem for the heat equation, whereas Borachok et al. [8] and Chapko and Johansson [9] developed a mesh-

less method of fundamental solutions and a boundary integral approach, respectively, for Cauchy problems for parabolic and hyperbolic equations. Other numerical procedures for obtaining accurate and stable solutions of Cauchy problems have also been devised, e.g. a generalized finite-difference method for the solution of the Cauchy problem for the Navier equations [5] in elasticity. Besides, Reinhardt et al. [6] and Berntsson et al. [7] coupled the conjugate gradient method (CGM) with Tikhonov regularization to obtain accurate and stable reconstructions for the solutions of the Cauchy problems for the heat and Helmholtz equations, respectively.

As far as wave propagation phenomena are concerned, research aiming towards solving Cauchy problems for hyperbolic equations was carried out in the past in [8,9,11–14]. The so-called quasi-reversibility method has been applied to solve the Cauchy problem for the wave equation [14–16]. This method's idea is to approximate the original ill-posed problem by a well-posed, but higher-order, problem for which analytical and numerical methods can be easily applied. Klibanov and Rakesh [14] used such a method to regularize the Cauchy problem for the wave equation subjected to lateral Cauchy data for smooth, bounded domains. Other related research was based on the use of mixed formulations of such an underlining method, see Bécache et al. [12] for details. Numerical methods have also been devised and applied [8,9,13]. For instance, the authors of [13] applied a hybrid boundary integral approach incorporating the Galerkin boundary element method to reconstruct an unknown boundary condition from lateral Cauchy data in the wave equation on a 3-D annulus. Worth mentioning here is also the analysis and solution of Weber [17] for the ill-posed inverse heat conduction problem obtained by approximating the parabolic heat equation with a hyperbolic damped wave equation with small parameter. Other applications of inverse analyses for hyperbolic equations concern source/force identification problems [18–20].

As far as the practical applications in the field of thermal biology are concerned, Yang [21] numerically estimated the skin temperature of a single-layered biological tissue from temperature measurements within the tissue by an inversion method based on a finite-element method incorporating the concept of future time steps, with extension to higher dimensions also attempted [22]. Lee et al. [23] utilized the thermal-wave model of bio-heat transfer and the CGM to accurately and stably recover the heat flux at the skin of a single-layered biological tissue. Hsu [22] combined a finite-difference method (FDM) with the linear least-squares method to identify the unspecified boundary conditions in a 3-D hyperbolic heat conduction model.

From the above literature review it can be concluded that inverse modelling is the appropriate approach to be employed when the data of interest are difficult or impossible to measure directly or when the corresponding devices and process of measuring is expensive and complicated. This conclusion justifies why it is important to solve the inverse problem of reconstructing the displacement at $x = 1$ from measurements of the displacement and flux at $x = 0$ for the one-dimensional wave equation in the domain $Q_T := (0, 1) \times (0, T)$ subjected to initial conditions at $t = 0$, as proposed in this paper. For $T > 1$, it is known that, due to the Holmgren unique continuation for the wave equation $u_{tt} - u_{xx} = 0$ in Q_T, the solution to

this Cauchy problem is unique only in the region:

$$R_T^0 = \{(x,t) \in Q_T | 0 < x < 1,\ 0 < t < T - x\}, \tag{1}$$

see [12] for more details. Even though the solution is unique in R_T^0, it may not exist if there is redundancy between the Cauchy and initial data at $t = 0$. In any case, it violates the stability condition [13, 14], i.e. small changes in the input data cause large changes in the output solution.

The next section presents the Cauchy problem for the one-dimensional wave equation.

2. Mathematical formulation

Consider the wave equation

$$u_{tt} - (a(x,t)u_x)_x = f(x,t), \quad (x,t) \in Q_T{=}(0,1) \times (0,T), \tag{2}$$

where $a(x,t)$ is the conductivity coefficient which is assumed positive, $u(x,t)$ represents the displacement and $f(x,t)$ is a force acting on the system. In defining the solution domain $Q_T = (0,1) \times (0,T)$ we have assumed, for simplicity, that the length of a vibrating string is equal to unity. Also, $0 < T < \infty$ stands for the duration of the time-horizon.

Associated with (2), we have prescribed the initial conditions

$$u(x,0) = u_0(x), \quad u_t(x,0) = v_0(x), \quad x \in (0,1), \tag{3}$$

on the displacement and velocity, and the Neumann flux boundary condition

$$-a(0,t)u_x(0,t) = \varphi(t), \quad t \in (0,T). \tag{4}$$

We consider the inverse problem consisting of reconstructing the unknown boundary displacement

$$u(1,t) = \psi(t), \quad t \in (0,T), \tag{5}$$

from the measurement of the boundary displacement

$$u(0,t) = \eta(t), \quad t \in (0,T). \tag{6}$$

To solve the inverse problem (2)-(4) and (6), we minimize the objective functional $J : L^2(0,T) \to \mathbb{R}_+$ defined by

$$J(\psi) := \frac{1}{2}\|u(0,t) - \eta^\epsilon(t)\|^2_{L^2(0,T)}, \tag{7}$$

where u solves (2)-(5) for a given element $\psi \in L^2(0,T)$, and $\eta^\epsilon(t)$ is the noisy measured boundary displacement, which satisfies

$$||\eta^\epsilon(t) - \eta(t)||_{L^2(0,T)} \leq \epsilon, \tag{8}$$

where $\epsilon \geq 0$ represents the amount of noise. As usual with iterative regularization methods, stopping the iterations in the minimization of (7) at an appropriate threshold given by the discrepancy principle plays the role of regularization. Alternatively, one could incorporate a regularization term $\lambda \|\psi(t)\|^2_{L^2(0,T)}$, where $\lambda > 0$ is the regularization parameter, directly into (7). It was demonstrated elsewhere, see [24], that both these regularization methods produce similar stable results in case of the inverse heat conduction problem (IHCP) for the parabolic heat equation.

We briefly recall the well-posedness of the direct problem (2)-(5). Data of the inverse problem can be contaminated with noise, hence we only require that the given functions are square integrable. Similar to what was done in [10] for parabolic equations, we consider the so-called very weak solution to (2)-(5), that is an element u satisfying

$$\begin{aligned} \int_0^T \int_0^1 u(x,t) \left(w_{tt} - (a(x,t)w_x)_x\right) dxdt \\ = \int_0^T \int_0^1 f(x,t)w(x,t)dxdt - \int_0^1 u_0(x)w_t(x,0)dx + \int_0^1 v_0(x)w(x,0)dx \\ + \int_0^T \varphi(t)w(0,t)dt - \int_0^T \psi(t) \left(a(1,t)w_x(1,t)\right) dt \end{aligned} \tag{9}$$

for every element w in $H^2(Q_T)$ satisfying $w(x,T) = w_t(x,T) = 0$ together with the mixed boundary conditions $a(0,t)w_x(0,t) = 0$ and $w(1,t) = 0$.

Following classical results of well-posedness and regularity, we assume that the coefficient a is positive and has a continuous derivative in each variable throughout the space-time cylinder Q_T, i.e. $a \in C^1(\overline{Q}_T)$ (in some parts considerable less smoothness works, for example, in the definition of a very weak solution $a \in L^\infty(Q_T)$ is enough). Then, following [10], we have: Given $f \in L^2(Q_T)$, u_0, $v_0 \in L^2(0,1)$ and φ, $\psi \in L^2(0,T)$, there exists a unique very weak solution $u \in L^2(Q_T)$ to (2)-(5) and the following *a priori* estimate holds:

$$\|u\|_{L^2(Q_T)} \leq C(\|f\|_{L^2(Q_T)} + \|u_0\|_{L^2(0,1)} + \|v_0\|_{L^2(0,1)} + \|\varphi\|_{L^2(0,T)} + \|\psi\|_{L^2(0,T)}). \tag{10}$$

It is possible to show regularity of this solution under suitable compatibility conditions using, for example, the standard Faedo-Galerkin ansatz; we refer to [25] for an overview of regularity results for solutions to the wave equation with Dirichlet, respectively Neumann, boundary conditions, and for mixed problems [26]; see also [27, Thm 8.1]. It is interesting to note, as pointed out in [25, Remarks 2.1] that, for the wave equation, there is so-called hidden regularity, meaning that smoothness on the lateral boundary can be shown although this does not follow from a trace theorem, see further [28]. A standard source of results for the wave equation in general form is [29, Chapter 3, Sections 8–9], see also the more recent work [30].

We finally remark that the problem where one and only one boundary condition of either Dirichlet or Neumann type is placed along each of the four sides of the space-time rectangle Q_T is only well-posed when the quotient of two different sides of the rectangle is an irrational number (uniqueness fails otherwise), see [31].

The structure of the remainder of the paper is as follows. In Section 3, we recast the inverse Cauchy problem under investigation as a variational problem and prove that the objective functional associated is Fréchet differentiable and derive a formula for its gradient. The CGM is then described for the minimization of the objective functional. Section 4 demonstrates the proposed inversion method and discusses its accuracy and stability for two numerical benchmark examples. The conclusions are highlighted in Section 5.

3. Variational problem

In this section, we prove that the objective functional defined in equation (7) is Fréchet differentiable and derive a formula for its gradient. In doing so, let us introduce the following adjoint problem to the problem given by (2)-(5):

$$v_{tt} - (a(x,t)v_x)_x = 0, \quad (x,t) \in Q_T, \tag{11}$$
$$v(x,T) = v_t(x,T) = 0, \quad x \in (0,1), \tag{12}$$
$$-a(0,t)v_x(0,t) = \eta^\epsilon(t) - u(0,t), \quad t \in (0,T), \tag{13}$$
$$v(1,t) = 0, \quad t \in (0,T). \tag{14}$$

Theorem 3.1. *The objective functional defined in* (7) *is Fréchet differentiable and its gradient is given by*

$$J'(\psi) = a(1,t)v_x(1,t), \quad t \in (0,T), \tag{15}$$

where $v(x,t)$ *is the solution of the adjoint problem given by equations* (11)-(14).

Proof. Taking a small variation $\Delta\psi \in L^2(0,T)$ of ψ, we have

$$J(\psi+\Delta\psi) - J(\psi) = \langle u(0,t;\psi) - \eta^\epsilon(t), \Delta u(0,t;\psi)\rangle_{L^2(0,T)} + \frac{1}{2}||\Delta u(0,t;\psi)||^2_{L^2(0,T)}, \tag{16}$$

where $\Delta u(x,t;\psi)$ is the solution of the sensitivity problem

$$(\Delta u)_{tt} - (a(x,t)(\Delta u)_x)_x = 0, \quad (x,t) \in Q_T, \tag{17}$$
$$\Delta u(x,0) = (\Delta u)_t(x,0) = 0, \quad x \in (0,1), \tag{18}$$
$$a(0,t)(\Delta u)_x(0,t) = 0, \quad t \in (0,T), \tag{19}$$
$$\Delta u(1,t) = \Delta\psi(t), \quad t \in (0,T). \tag{20}$$

From the *a priori* estimate (10) for the sensitivity problem (17)-(20), we have

$$||\Delta u(0,t;\psi)||^2_{L^2(0,T)} = o\left(\|\Delta\psi\|_{L^2(0,T)}\right), \quad \text{as } \|\Delta\psi\|_{L^2(0,T)} \to 0. \tag{21}$$

Moreover, multiplying (11) by $\Delta u(x,t)$ and integrating by parts twice, using (12)-(20), yield

$$\int_0^T (u(0,t;\psi) - \eta^\epsilon(t))\Delta u(0,t;\psi)dt = \int_0^T a(1,t)v_x(1,t)\Delta\psi(t)dt. \tag{22}$$

Therefore, equation (16) becomes

$$J(\psi+\Delta\psi) - J(\psi) = \int_0^T a(1,t)v_x(1,t)\Delta\psi(t)dt + o\left(\|\Delta\psi\|_{L^2(0,T)}\right). \tag{23}$$

From the right-hand side of the above equation and the definition of the Fréchet derivative, we see that $J(\psi)$ is Fréchet differentiable and its gradient at ψ is given by (15).

In the next subsection, the CGM is described for the minimization of the objective functional defined in (7).

3.1 Iterative procedure

To find the unique minimizer of the objective functional defined in equation (7) we employ the CGM given by the recursive relations

$$\psi^{n+1} = \psi^n - \alpha_n d_n, \quad n = 0, 1, \ldots, \tag{24}$$

where the direction of descent d_n is given by

$$d_n = \begin{cases} -J'(\psi^n), & \text{if } n = 0, \\ -J'(\psi^n) + \beta_n d_{n-1}, & \text{if } n = 1, 2, \ldots, \end{cases} \tag{25}$$

the Fletcher–Reeves conjugate coefficient β_n is given by [32]

$$\beta_0 = 0, \qquad \beta_n = \frac{\|J'(\psi^n)\|^2_{L^2(0,T)}}{\|J'(\psi^{n-1})\|^2_{L^2(0,T)}}, \quad n = 1, 2, \ldots, \tag{26}$$

and the search step size α_n is computed as the minimizer

$$\alpha_n = \underset{\alpha \geq 0}{\operatorname{argmin}}\ J(\psi^n - \alpha d_n), \quad n = 0, 1, \ldots. \tag{27}$$

Other choices for β_n such as the Polak-Ribiere [33], Hestenes-Stiefel [34] or Dai-Yuan [35] can also be adopted.

In (25), d_0 is $-J'(\psi^0)$, so the usual gradient descent method requires moving in the direction of the negative gradient of J at ψ^0. For $n \geq 1$ however, we insist that the directions d_n be conjugate to each other in order to enforce the iteration to follow narrow valleys in regions where the steepest descent would otherwise slow down.

To evaluate α_n, we set $\Delta\psi^n = d_n$ and linearize $u(0, t; \psi^n - \alpha d_n)$ by a first-order Taylor series expression to obtain

$$u(0, t; \psi^n - \alpha d_n) \approx u(0, t; \psi^n) - \alpha d_n \frac{\partial u}{\partial \psi^n}(0, t; \psi^n) \approx u(0, t; \psi^n) - \alpha \Delta u(0, t; \psi^n), \tag{28}$$

where $\Delta u(0, t; \psi^n)$ is found by solving the sensitivity problem (17)-(20) with $\Delta\psi^n = d_n$. Then, differentiating $J(\psi^n - \alpha d_n)$ with respect to α and making it zero yield

$$\alpha_n = \frac{\langle u(0, t; \psi^n) - \eta^\epsilon(t), \Delta u(0, t; \psi^n) \rangle_{L^2(0,T)}}{\|\Delta u(0, t; \psi^n)\|^2_{L^2(0,T)}}. \tag{29}$$

3.2 Stopping criterion

For stability, we stop the iterations according to the discrepancy principle, i.e. we stop the iterations at the first iteration n_* for which, according to (7) and (8),

$$J(\psi^{n_*}) \approx \epsilon^2/2 =: \bar{\epsilon}. \tag{30}$$

For exact data, we stop the iterative procedure at the first iteration n_* for which $J(\psi^{n_*})$ attains a small positive value such as 10^{-5}.

3.3 Algorithm

The CGM's steps are summarized as follows:

1. Set $n = 0$ and select an arbitrary initial guess $\psi^0 \in L^2(0, T)$.
2. Solve the direct problem given by equations (2)-(5) to obtain $u(x, t; \psi^n)$ and compute $J(\psi^n)$ from equation (7).
3. Stop if the stopping criterion (30) is satisfied. Else go to step 4.
4. Solve the adjoint problem given by equations (11)-(14) to find $v(x, t; \psi^n)$. Compute the gradient $J'(\psi^n)$ from equation (15), the conjugate coefficient β_n from equation (26), and the direction of descent d_n from equation (25).
5. Solve the sensitivity problem given by equations (17)-(20) to obtain $\Delta u(x, t; \psi^n)$ by taking $\Delta\psi^n = d_n$ and compute the search step size α_n from equation (29).
6. Update ψ^{n+1} from equation (24), set $n = n + 1$ and go to step 2.

4. Numerical results and discussion

In the numerical examples below, we use the FDM, as in [36], based on the unconditionally stable Crank-Nicolson scheme with uniform mesh size $\Delta x = 1/M$ and time step $\Delta t = T/N$, to solve the direct, adjoint and sensitivity problems present in the CGM described in Section 3.3. The trapezoidal rule is used for discretizing the integrals in equations (26) and (29). The accuracy error functional, as a function of the number of iterations n, is defined as

$$E(\psi^n) = ||\psi^n - \psi||_{L^2(0,T-1)}, \tag{31}$$

where ψ^n stands for the numerical result obtained by the CGM at the iteration number n and ψ denotes the true boundary displacement defined in equation (5), if available.

The noisy data $\eta^\epsilon(t)$ is simulated by adding random noise to the exact data $\eta(t)$, as follows:

$$\eta^\epsilon(t_j) = \eta(t_j) + \epsilon_j, \quad j = \overline{1, N}, \tag{32}$$

where $t_j = j\Delta t$ for $j = \overline{0, N}$ are the FDM time nodes and ϵ_j for $j = \overline{1, N}$ are N random variables generated from a Gaussian normal distribution with mean zero and standard deviation $\sigma = p \times \max_{t\in[0,T]} |\eta(t)|$, where p represents the percentage of noise. We use the MATLAB function $normrnd(0, \sigma, N)$ to generate the random variables $(\epsilon_j)_{j=\overline{1,N}}$.

In the next two subsections, we present two numerical examples to verify the accuracy and stability of the proposed CGM. As pointed out at the end of section 1, in case of constant coefficient $a(x, t)$, the uniqueness of a solution of the Cauchy problem (2)-(4) and (6) holds only in the region R_T^0 defined in (1). Explicit uniqueness results for the general case of a non-constant $a(x, t)$ are not known at present, although some sidewise profile control has

very recently been attempted in [37] for the wave equation $\rho(x)u_{tt} - (a(x)u_x)_x = 0$ with space-dependent uniformly bounded positive coefficients $\rho(x)$ and $a(x)$.

We take $T = 2$ and then, according to the theory [12], the solution for the boundary displacement (5) at $x = 1$ can be uniquely identified only for $t \in (0, 1)$, which is obtained from (1) with $x = 1$ and $T = 2$.

4.1 Example 1

In this example, we take the input data

$$a(x,t) = 1, \quad u(x,0) = u_0(x) = 1 + x, \quad u_t(x,0) = v_0(x) = 1 + x, \quad f(x,t) = (1+x)e^t, \tag{33}$$

$$-a(0,t)u_x(0,t) = \varphi(t) = -e^t, \tag{34}$$

and consider the boundary displacement

$$u(0,t) = \eta(t) = e^t. \tag{35}$$

It can be verified by direct substitution that the analytical solution of the inverse problem given by equations (2)-(4) and (6) is

$$u(x,t) = (1+x)e^t, \quad u(1,t) = \psi(t) = 2e^t. \tag{36}$$

From the theory, we already know that $u(1,t)$ can be retrieved uniquely only in the interval $t \in (0,1)$ from the Cauchy data (34) and (35). We take the initial guess $\psi_1^0(t) = (e^2-1)t+2$ as well as $\psi_2^0(t) = 2(e-1)t+2$, and run the CGM described in Section 3.3 with $\Delta t = \Delta x = 0.025$ for 10 iterations. Both these initial guesses are linear functions of t, while the exact solution for $\psi(t)$ is an exponential function. The first initial guess satisfies $\psi_1^0(0) = \psi(0)$ and $\psi_1^0(2) = \psi(2)$, while the second initial guess satisfies $\psi_2^0(0) = \psi(0)$ and $\psi_2^0(1) = \psi(1)$. Since the initial guess ψ_2^0 equals the exact solution at $t = 1$ we expect to obtain a better convergence and numerical results for it compared to the initial guess ψ_1^0. This conclusion is clearly illustrated in Figures 1(a) and (b), which show the monotonic decreasing convergence of the objective functional $J(\psi^n)$ and the accuracy error functional $E(\psi^n)$, respectively, as functions of the number of iterations n, starting from the initial guesses $\psi_1^0(t)$ and $\psi_2^0(t)$ for exact data, i.e. $p = 0$.

Figures 2(a) and (b) present the corresponding numerical solutions for the unknown boundary displacement $\psi(t)$ alongside the exact solution (36) starting from $\psi_1^0(t)$ for $t \in [0,2]$ and $t \in [0,1]$, respectively. Similar results to those reported in Figures 2(a) and (b) are depicted in Figures 2(c) and (d), but starting from $\psi_2^0(t)$. As discussed before, uniqueness can be ensured only on the time interval $t \in (0,1)$, as illustrated in Figures 2(a) and (c). Moreover, the results obtained with the initial guess $\psi_2^0(t)$ presented in Figure 2(d) are more accurate and stable than those obtained with the initial guess $\psi_1^0(t)$ presented in Figure 2(b).

Next, we consider noisy input data with $p \in \{1, 10\}\%$ noise. We present results only for the initial guess $\psi_2^0(t) = 2(e-1)t + 2$. The monotonic decreasing convergence of the objective functional $J(\psi^n)$ and the accuracy error functional $E(\psi^n)$, as functions of the number of iterations n, are presented in Figures 3(a) and (b), respectively. As expected, these curves

attain lower values for $p = 1\%$ noise than for the higher amount of noise $p = 10\%$ with which the input boundary displacement data (32) is contaminated. The graphs in Figure 3(b) also show that there is a minimum (at iteration number $n = 2$) in the accuracy error (31), which is attained close to the iteration number $n_* = 1$ given by the discrepancy principle (30), as illustrated in Figure 3(a). The corresponding reconstructions of the unknown boundary displacement $\psi(t)$ obtained at the stopping iteration number $n_* = 1$ are presented in Figure 4 in comparison with the exact solution (36). From this figure it can be seen that the numerical results obtained for $p = 1\%$ noise are accurate and stable, but for the higher amount of $p = 10\%$ noise some mild oscillations start to become visible.

4.2 Example 2

We take the input data

$$a(x,t) = 1, \quad u(x,0) = u_0(x) = 0, \quad u_t(x,0) = v_0(x) = \pi\cos(\pi x), \quad f(x,t) = 0, \tag{37}$$

$$-a(0,t)u_x(0,t) = \varphi(t) = 0, \tag{38}$$

and consider the boundary displacement

$$u(0,t) = \eta(t) = \sin(\pi t). \tag{39}$$

It can be verified by direct substitution that the analytical solution of the inverse problem given by equations (2)-(4) and (6) is

$$u(x,t) = \sin(\pi t)\cos(\pi x), \quad u(1,t) = \psi(t) = -\sin(\pi t). \tag{40}$$

We take the initial guess $\psi^0(t) = 0$ and run the CGM described in Section 3.3 with $\Delta t = \Delta x = 0.025$ for 10 iterations. Figures 5(a) and (b) show the monotonic decreasing convergence of the objective functional $J(\psi^n)$ and the accuracy error functional $E(\psi^n)$, respectively, as functions of the number of iterations n, for exact data, i.e. $p = 0$. Figure 6 illustrates the very good agreement between the numerical solution for the boundary displacement $\psi(t)$ for $t \in [0,1]$, in comparison with the exact solution (40).

Next, we consider noisy input data with $p \in \{1, 20\}\%$ noise. The monotonic decreasing convergence of the objective functional $J(\psi^n)$ and the accuracy error functional $E(\psi^n)$, as functions of the number of iterations n, are presented in Figures 7(a) and (b), respectively. As for Example 1, it can be seen that there is a close correlation between the minimum of the error curves (obtained after 2 iterations), as illustrated in Figure 7(b), and the stopping iteration numbers $n_* \in \{2, 1\}$ for $p \in \{1, 20\}\%$, respectively, as illustrated in Figure 7(a). The corresponding reconstructions of the unknown boundary displacement $\psi(t)$ obtained at these stopping iteration numbers of $n_* \in \{2, 1\}$ for $p \in \{1, 20\}\%$, respectively, are presented in Figure 8 in comparison with the exact solution (40). As for Example 1, it can be seen that the numerical results obtained for $p = 1\%$ noise are accurate and stable, but for the higher amount of $p = 20\%$ noise some mild oscillations start to manifest.

5. Conclusions

In the present paper, a Cauchy problem associated with the wave equation has been solved

by using the CGM. This linear but ill-posed inverse problem, reformulated as a least-squares minimization problem, consists of finding the displacement on a hostile and inaccessible part of the medium boundary from measurements of the Cauchy data on the remaining friendly and accessible part of the boundary. For a one-dimensional vibrating string of unit length, the uniqueness of the boundary displacement at $x = 1$ holds only over the restricted time interval $t \in (0, T-1)$, where $T > 1$. The solution $u(1,t)$ is not unique for $t \in [T-1, T]$ and the numerically obtained results confirm this feature of the ill-posed Cauchy problem for the wave equation.

The associated least-squares objective functional has been proved to be Fréchet differentiable and a formula for its gradient has been derived. A minimization procedure based on the CGM has been proposed and applied for the iterative minimization of the objective functional with the discrepancy principle employed for obtaining stable solutions. The well-posed problems: the direct, adjoint and sensitivity problems present in the CGM have been discretized by using a FDM. To verify the accuracy and stability of the proposed inversion method, numerical results for two benchmark examples have been thoroughly presented and discussed. These results illustrate the very fast convergence of the CGM in less than 10 iterations for exact data. Furthermore, the iterative method is proved to be remarkably stable if stopped according to the discrepancy principle, even when high amounts of $10\% - 20\%$ noisy data are inverted.

When the initial conditions (3) are not prescribed, the solution of the wave equation $u_{tt} - u_{xx} = 0$ in Q_T subject to the Cauchy data $u(0,t) = \eta(t)$ and $-u_x(0,t) = \varphi(t)$ for $t \in (0,T)$ is unique only in the restricted subset $R_T = \{(x,t) \in Q_T | 0 < x < 1,\ x < t < T - x\} \subset R_T^0$ for $T > 2$, see [12]. However, even for this more ill-posed Cauchy problem for the hyperbolic wave equation without initial conditions the CGM can still be applied by extending the analyses of [3, 38] for the parabolic heat equation without initial data.

The proposed CGM of this study is also applicable to other kinds of applied inverse problems for hyperbolic equations such as source estimation in the non-Fourier regime of heat transfer in biological bodies.

Acknowledgements
M. Alosaimi would like to thank Taif University in Saudi Arabia and the United Kingdom Saudi Arabian Cultural Bureau (UKSACB) in London for supporting his PhD studies at the University of Leeds.

References

[1] Hào DN, Lesnic D. The Cauchy problem for Laplace's equation via the conjugate gradient method. IMA J Appl Math. 2000;65:199–217.

[2] Tuan NH, Binh TT, Viet TQ, et al. On the Cauchy problem for semilinear elliptic equations. J Inverse Ill-Posed Probl. 2016;24:123–138.

[3] Hào DN. A noncharacteristic Cauchy problem for linear parabolic equations II: a variational method. Numer Funct Anal Optim. 1992;13:541–564.

[4] Horáček BM, Clements JC. The inverse problem of electrocardiography: a solution in terms of single- and double-layer sources on the epicardial surface. Math Biosci. 1997;144:119–154.

[5] Li P-W, Fu Z-J, Gu Y, et al. The generalized finite difference method for the inverse Cauchy problem in two-dimensional isotropic linear elasticity. Int J Solids Struct. 2019;174–175:69–84.

[6] Reinhardt H-J, Hào DN, Frohne J, et al. Numerical solution of inverse heat conduction problems in two spatial dimensions. J Inverse Ill-Posed Probl. 2007;15:181–198.

[7] Berntsson F, Kozlov VA, Mpinganzima L, et al. Iterative Tikhonov regularization for the Cauchy problem for the Helmholtz equation. Comput Math Appl. 2017;73:163–172.

[8] Borachok I, Chapko R, Johansson BT. A method of fundamental solutions for heat and wave propagation from lateral Cauchy data. To appear in Numerical Algorithms; 2021. Doi: 10.1007/s11075-021-01120-x.

[9] Chapko R, Johansson BT. A boundary integral equation method for numerical solution of parabolic and hyperbolic Cauchy problems. Appl Numer Math. 2018;129:104–119.

[10] Bastay G, Kozlov VA, Turesson BO. Iterative methods for an inverse heat conduction problem. J Inverse Ill-Posed Probl. 2001;9:375–388.

[11] Amirov A, Yamamoto M. A timelike Cauchy problem and an inverse problem for general hyperbolic equations. Appl Math Lett. 2008;21:885–891.

[12] Bécache E, Bourgeois L, Franceschini L, et al. Application of mixed formulations of quasi-reversibility to solve ill-posed problems for heat and wave equations: the 1D case. Inverse Probl Imaging. 2015;9:971–1002.

[13] Chapko R, Johansson BT, Muzychuk Y, et al. Wave propagation from lateral Cauchy data using a boundary element method. Wave Motion. 2019;91:102385.

[14] Klibanov MV, Rakesh. Numerical solution of a time-like Cauchy problem for the wave equation. Math Meth Appl Sci. 1992;15:559–570.

[15] Klibanov MV. Carleman estimates for the regularization of ill-posed Cauchy problems. Appl Numer Math. 2015;94:46–74.

[16] Klibanov MV, Timonov AA. Carleman Estimates for Coefficient Inverse Problems and Numerical Applications. Berlin: De Gruyter; 2019.

[17] Weber CF. Analysis and solution of the ill-posed inverse heat conduction problem. Int J Heat Mass Transf. 1981;24:1783–1792.

[18] Clason C, Klibanov MV. The quasi-reversibility method for thermoacoustic tomography in a heterogeneous medium. SIAM J Sci Comput. 2007;30:1–23.

[19] Lesnic D, Hussein SO, Johansson BT. Inverse space-dependent force problems for the wave equation. J Comput Appl Math. 2016;306:10–39.

[20] Nguyen LH. An inverse space-dependent source problem for hyperbolic equations and the Lipschitz-like convergence of the quasi-reversibility method, Inverse Probl. 2019;35:035007.

[21] Yang C-Y. Boundary estimation of hyperbolic bio-heat conduction. Int J Heat Mass Transf. 2011;54:2506–2513.

[22] Hsu P-T. Estimating the boundary condition in a 3D inverse hyperbolic heat conduction problem. Appl Math Comput. 2006;177:453–464.

[23] Lee H-L, Lai T-H, Chen W-L, et al. An inverse hyperbolic heat conduction problem in estimating surface heat flux of a living skin tissue. Appl Math Model. 2013;37:2630–2643.

[24] Hào DN, Thành PX, Lesnic D, et al. A boundary element method for a multi-dimensional inverse heat conduction problem. Int J Comput Math. 2012;89:1540–1554.

[25] Lasiecka I, Triggiani R. Recent advances in regularity of second-order hyperbolic mixed problems, and applications. In: CKRT Jones, U Kirchgraber, HO Walther (Eds.). Dynamics Reported-Expositions in Dynamical Systems. Vol. 3. Berlin: Springer-Verlag; 1994. p. 104–162.

[26] Bennish J. The mixed Dirichlet-Neumann-Cauchy problem for second order hyperbolic operators. J Math Anal Appl. 1997;209:243–254.

[27] Isakov V. Inverse Problems for Partial Differential Equations. Berlin: Springer-Verlag; 2017.

[28] Bociu L, Zolésio J-P. A pseudo-extractor approach to hidden boundary regularity for the wave equation with mixed boundary conditions, J Differ Equ. 2015;259:5688–5708.

[29] Lions JL, Magenes E. Non-Homogeneous Boundary Value Problems and Applications. Vol. 1. Berlin: Springer-Verlag; 1972.

[30] Ikawa M. Hyperbolic Partial Differential Equations and Wave Phenomena. Providence (RI): American Mathematical Society; 2000.

[31] Abdul-Latif AI, Diaz JB. Dirichlet, Neumann, and mixed boundary value problems for the wave equation $u_{xx} - u_{yy} = 0$ for a rectangle. Appl Anal. 1971;1:1–12.

[32] Fletcher R, Reeves CM. Function minimization by conjugate gradients. Comput J. 1964;7:149–154.

[33] Polak E, Ribiere G. Note sur la convergence de methodes de directions conjuguees. Rev Fr Inf Rech Opér. 1969;3:35–43.

[34] Hestenes MR, Stiefel E. Methods of conjugate gradients for solving linear systems. J Res Natl Bur Stand. 1952;49:409–436.

[35] Dai YH, Yuan Y. A nonlinear conjugate gradient method with a strong global convergence property. SIAM J Optim. 1999;10:177–182.

[36] Dai W, Nassar R. A finite difference scheme for solving the heat transport equation at the microscale. Numer Meth Part Differ Equ. 1999;15:697–708.

[37] Saraç Y, Zuazua E. Sidewise profile control of 1-D waves. arXiv preprint arXiv: 2101.00473v3; 2021.

[38] Hào DN, Thành NT, Sahli H. Splitting-based conjugate gradient method for a multi-dimensional linear inverse heat conduction problem. J Comput Appl Math. 2009;232:361–377.

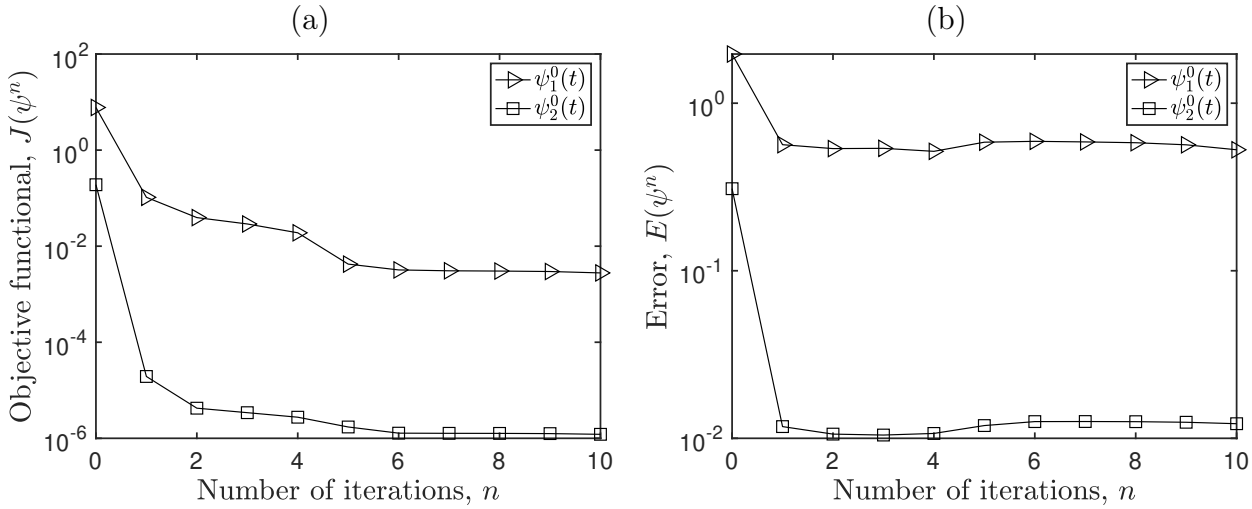

Figure 1: (a) The objective functional $J(\psi^n)$ and (b) the accuracy error functional $E(\psi^n)$, with $p = 0$, for Example 1, starting from the initial guesses $\psi_1^0(t)$ and $\psi_2^0(t)$.

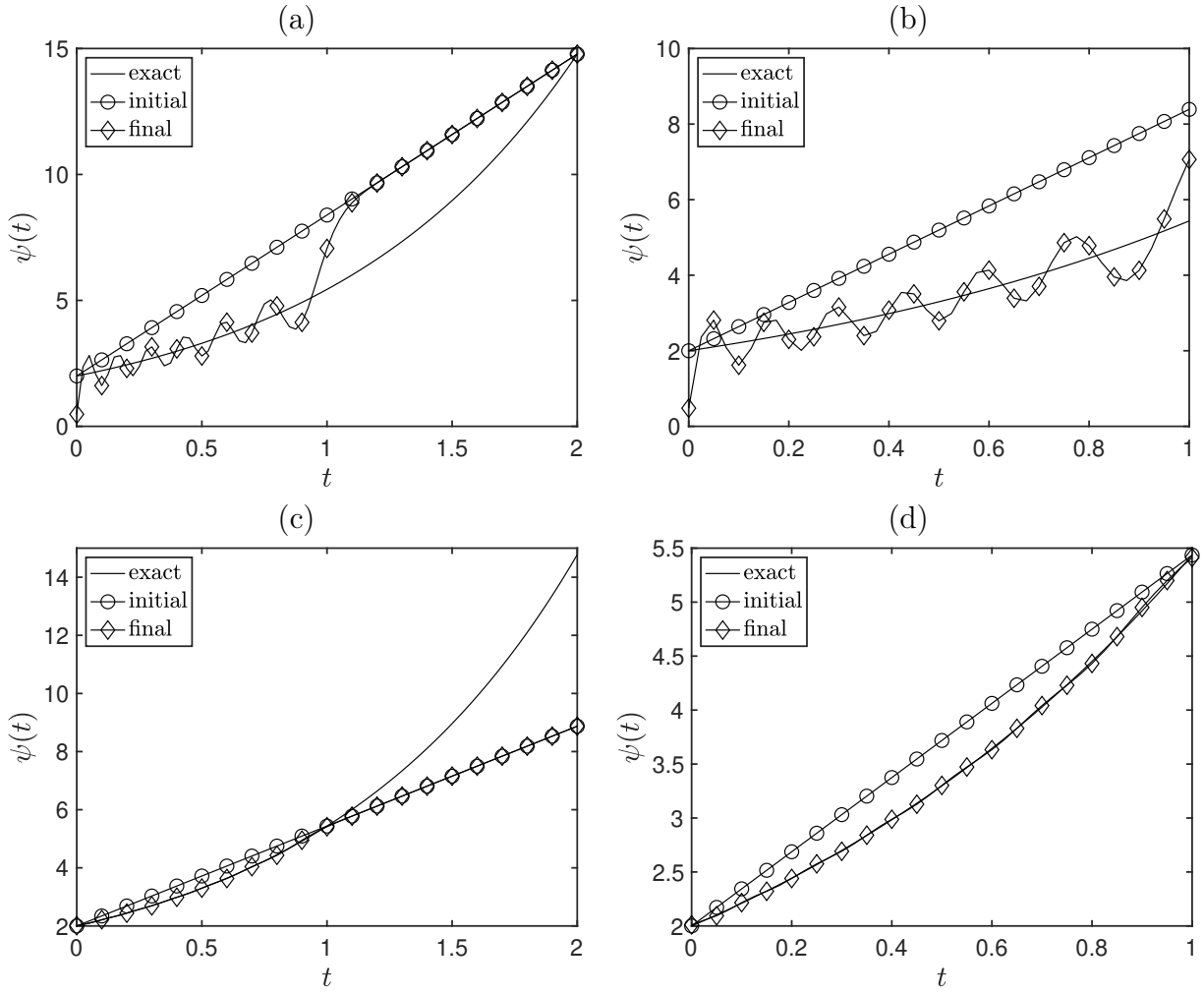

Figure 2: The analytical (36) and numerical boundary displacement $\psi(t)$ for (a) $t \in [0, 2]$ and (b) $t \in [0, 1]$, starting from the initial guess $\psi_1^0(t)$, with $p = 0$, for Example 1. Similar results to (a) and (b) are presented in (c) and (d), but starting from the initial guess $\psi_2^0(t)$. Results in (c) and (d) are very accurate for $t \in [0, 1]$, whilst the results in (a) and (b) starting from the initial guess $\psi_1^0(t)$ manifest some instabilities.

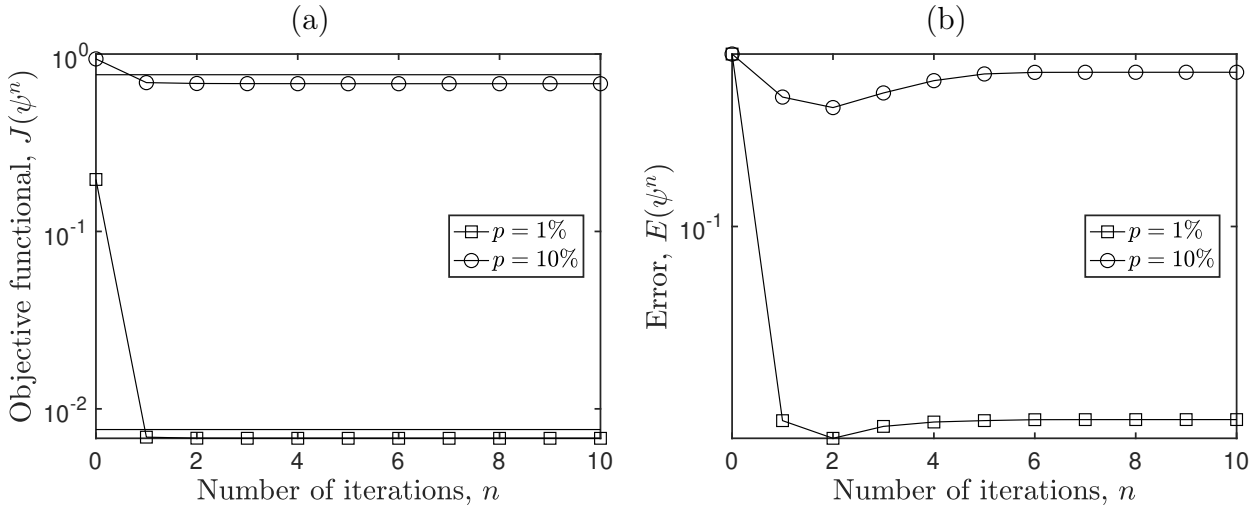

Figure 3: (a) The objective functional $J(\psi^n)$ along with the horizontal lines $y = \bar{\epsilon}$, and (b) the accuracy error functional $E(\psi^n)$, with $p \in \{1, 10\}\%$ noise, for Example 1, starting from the initial guess $\psi_2^0(t)$.

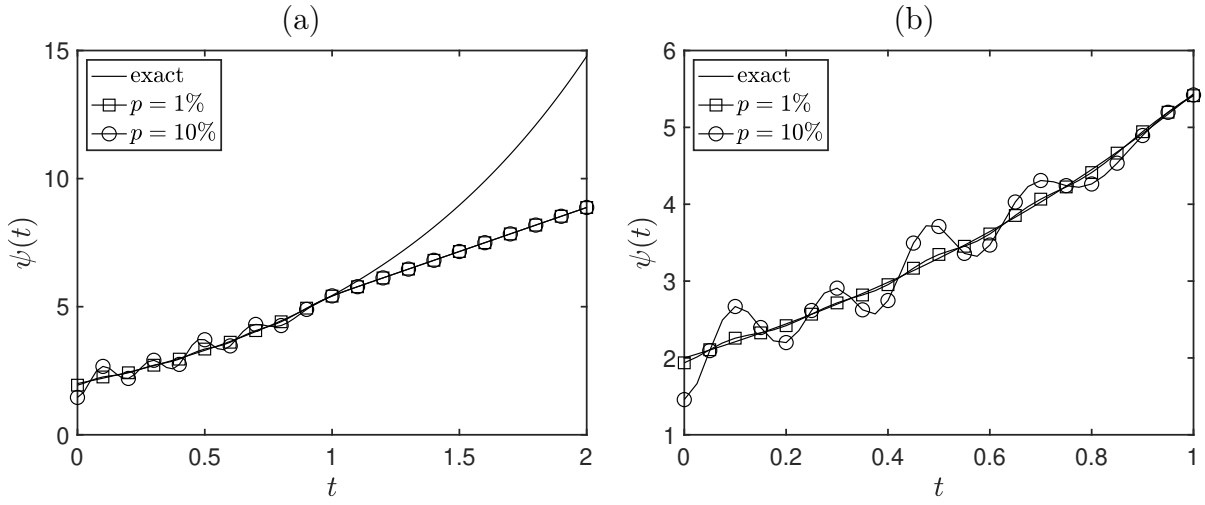

Figure 4: The analytical (36) and numerical boundary displacement $\psi(t)$ for (a) $t \in [0, 2]$ and (b) $t \in [0, 1]$, with $p \in \{1, 10\}\%$ noise, for Example 1, starting from the initial guess $\psi_2^0(t)$. The results are accurate and reasonably stable for $t \in [0, 1]$.

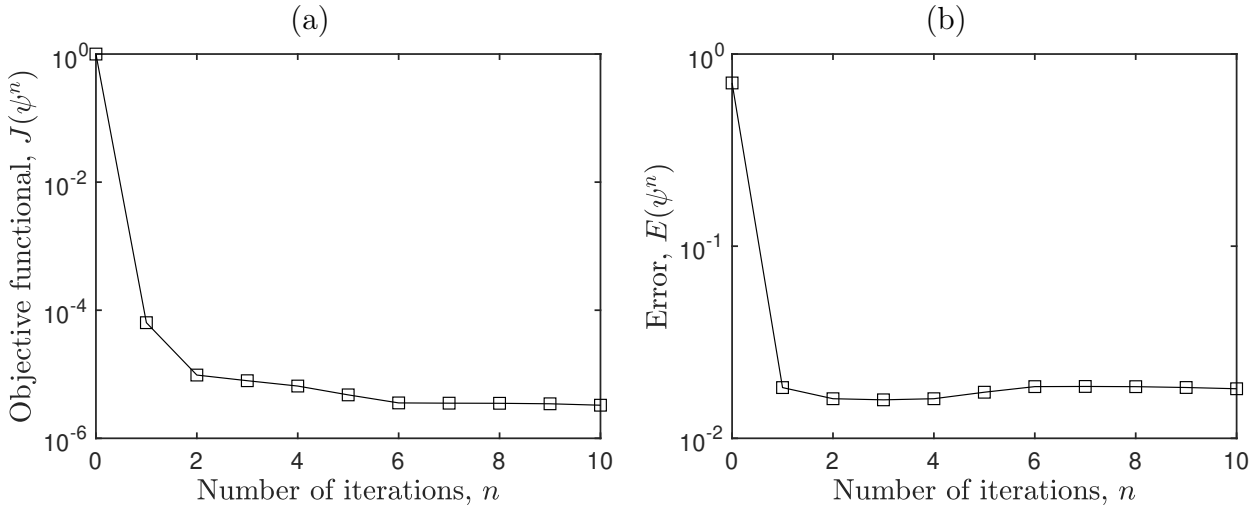

Figure 5: (a) The objective functional $J(\psi^n)$ and (b) the accuracy error functional $E(\psi^n)$, with $p = 0$, for Example 2.

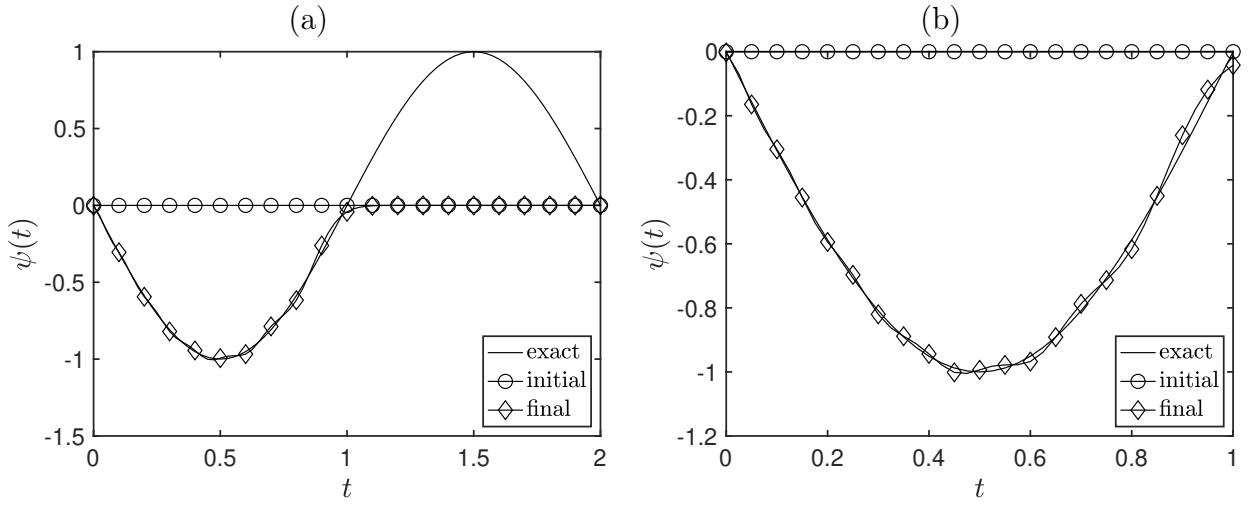

Figure 6: The analytical (40) and numerical boundary displacement $\psi(t)$ for (a) $t \in [0, 2]$ and (b) $t \in [0, 1]$, with $p = 0$, for Example 2.

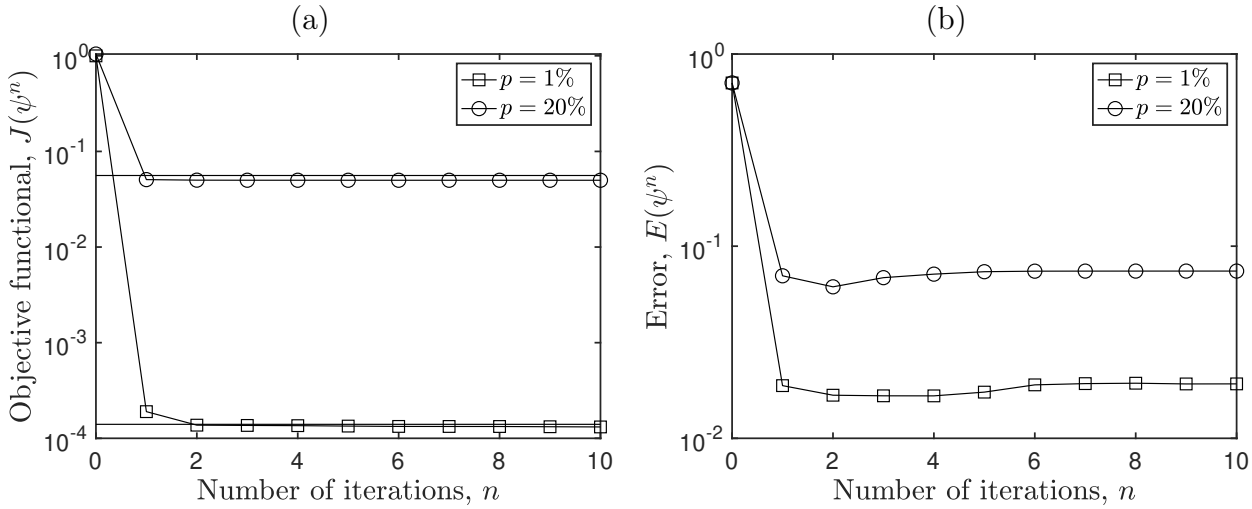

Figure 7: (a) The objective functional $J(\psi^n)$ along with the horizontal lines $y = \bar{\epsilon}$ and (b) the accuracy error functional $E(\psi^n)$, with $p \in \{1, 20\}\%$ noise, for Example 2.

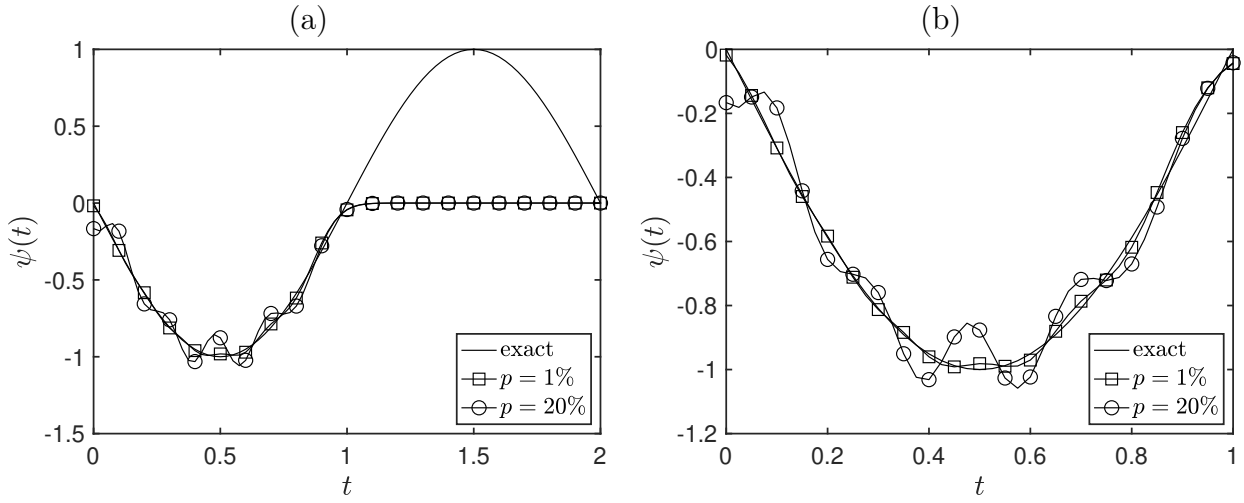

Figure 8: The analytical (40) and numerical boundary displacement $\psi(t)$ for (a) $t \in [0, 2]$ and (b) $t \in [0, 1]$, with $p \in \{1, 20\}\%$ noise, for Example 2.